Multi-Objective Design Optimization of Antennas for Reflection, Size and Gain Variability Using Kriging Surrogates and Generalized Domain Segmentation

Slawomir Koziel[1,2], Adrian Bekasiewicz[2] and Stanislaw Szczepanski[2]

[1]Engineering Optimization & Modeling Center, Reykjavik University
Reykjavik, Iceland, koziel@ru.is

[2]Faculty of Electronics, Telecommunications and Informatics, Gdansk University of Technology, Gdansk, Poland, bekasiewicz@ru.is, stanisla@eti.pg.gda.pl

Abstract

Cost-efficient multi-objective design optimization of antennas is presented. The framework exploits auxiliary data-driven surrogates, a multi-objective evolutionary algorithm for initial Pareto front identification, response correction techniques for design refinement, as well as generalized domain segmentation. The purpose of this last mechanism is to reduce the volume of the design space region that needs to be sampled in order to construct the surrogate model, and, consequently, limit the number of training data points required. The recently introduced segmentation concept is generalized here to allow for handling an arbitrary number of design objectives. Its operation is illustrated using a ultra-wideband monopole optimized for best in-band reflection, minimum gain variability, and minimum size. Compared to conventional surrogate-based approach, segmentation leads to reduction of the initial Pareto identification cost by over 20 percent. Numerical results are supported by experimental validation of the selected Pareto-optimal antenna designs.

1. Introduction

Design of modern antennas faces multiple challenges. These include the necessity of satisfying strict performance specifications that concern both electrical and field properties, size limitations, or high cost of computational models (full-wave EM analysis is normally required for reliable antenna evaluation). Other issues are related to a large number of adjustable parameters (being a consequence of geometrical complexity of today's antennas), as well as requirements to implement non-standard characteristics (e.g., band notches in case of wideband antennas). Many of performance requirements stay in conflict with each other so that improvement of them leads to degradation of the others. A relevant example is design of miniaturized wideband antennas, where—assuming fixed topology of the structure—reduction of the physical dimensions results in limiting the impedance bandwidth [1], increased gain variability or degradation of pulse stability [2]. On the other hand, a mere handling of several design goals is difficult or even impossible when using conventional methods such as parameter sweeping. In practice, it is often realized in a simplistic manner, e.g., by selecting a primary objective and controlling others using implicit [3] or explicit constraints [4]. This enables utilization of traditional optimization algorithms although does not allow for obtaining comprehensive information about available design trade-offs.

In most cases reported in the literature, in the context of design closure, antenna optimization is conducted in a single-objective regime. Usually, a structure topology is first established (often by introducing several consecutive geometry modifications), followed by a parameter tuning. If the adjustment process is based on parameter sweeping, a single performance figure can be controlled directly (e.g., impedance

bandwidth), whereas others are handled implicitly or are just byproducts of topology selection (e.g., [5]-[7]). Rigorous numerical optimization offers much better control over multiple antenna characteristics [8], [9]. However, due to high cost of EM simulation, conventional optimization algorithms [10] may be prohibitively expensive. This is particularly pronounced for population-based metaheuristics (genetic/evolutionary algorithms, particle swarm optimizers [11]-[14]). There have been numerous techniques developed to speed up the optimization process. Popular methods include utilization of adjoint sensitivities [15], [16], as well as surrogate-assisted techniques [17]-[20]. Surrogate-based optimization (SBO) is founded on the idea of shifting the optimization burden into a faster representation of the structure under design (the surrogate), which can be based on auxiliary data-driven models [21] or coarse-discretization EM simulations [17].

It is multi-objective optimization (MOO) that provides the most comprehensive information about the antenna structure and its capabilities in the context of a particular set of performance figures. MOO aims at finding a so-called Pareto set which represents the best possible trade-offs between the considered design objectives. By far, the most popular MOO techniques up to date are population-based metaheuristics [11]-[13]. The fundamental advantage of this class of techniques is their ability to generate the entire Pareto set in a single algorithm run [22]. Although initially limited to genetic algorithms, currently, pretty much all major metaheuristic algorithms have their multi-objective versions. Pushing the population of candidate solutions into the Pareto front is achieved by introducing appropriate selection procedures (e.g., Pareto-ranking-based ones), as well as other mechanisms (e.g., fitness sharing) that reduce formation of clusters. A principal

disadvantage of metaheuristics is high computational cost. Typically, thousands and tens of thousands of objective function evaluations are necessary for the algorithm to converge. If full-wave EM analysis is utilized for antenna evaluation, such a large number of simulations is clearly unacceptable.

Reduction of the MOO cost can be obtained by means of surrogate-based approaches, often involving both data-driven and physics-based models in the same optimization framework. A technique involving variable-fidelity EM simulations and auxiliary kriging interpolation models has been proposed in [23]. One of the issues is the necessity of constructing quasi-global surrogates because MOO normally implies global search. Due to curse of dimensionality this is becomes a problem for higher-dimensional parameter spaces. In order to alleviate this difficulty, design space reduction techniques have been introduced in [24] and [25]. These methods are capable of yielding Pareto sets at the costs corresponding to only a few hundred evaluations of the high-fidelity EM simulations of the antenna structure at hand, and handling highly-dimensional cases (> 20 parameters). In [26], a design space segmentation has been introduced with the purpose of reducing the number of samples necessary to construct the kriging surrogate model for the method [14]. As indicated by the results obtained in [26], this leads to further reduction of the CPU cost of MOO. The main idea behind segmentation is to define—based on appropriately allocated intermediate points—sub-domains that still cover the entire Pareto front but their total volume is significantly smaller than that of the original design space. A disadvantage of the approach [26] is that it only works for two design objectives. In this work, the segmentation approach is generalized to an arbitrary number of objectives. Our technique is demonstrated using an ultra-wideband monopole antenna optimized with

respect to three objectives: minimization of in-band reflection, minimization of gain variability, and reduction of the antenna size. Numerical results indicate that segmentation leads to over 20-percent reduction of the cost of initial Pareto set identification. Experimental validation of selected Pareto-optimal designs is also provided.

2. Surrogate-Based Multi-Objective Optimization

The design process is executed at the level of the primary computational model of the antenna structure at hand, used to evaluate its performance parameters. Here, it is a high-fidelity EM simulation model $R_f(x)$. A vector x represents designable parameters. The aim is to simultaneously minimize N_{obj} objectives $F_k(R_f(x))$, $k = 1, \ldots, N_{obj}$. In multi-objective design, the two designs x and y can be compared using a dominance relation $\prec$ defined as follows: $y \prec x$ (or y dominates over x) if $F_k(R_f(y)) \leq F_k(R_f(x))$ for all $k = 1, \ldots, N_{obj}$, and $F_k(R_f(y)) < F_k(R_f(x))$ for at least one k [22]. The optimum designs are those that are not dominated by any other designs within the search space. In a typical case of partially conflicting objectives, the Pareto front (the set consisting of Pareto-optimal designs) is an $N_{obj} - 1$ dimensional manifold in the objective space. The goal of multi-objective optimization is to identify a discrete representation of it, referred to as a Pareto set. The Pareto set represents the best possible trade-offs between objectives F_k.

A surrogate-assisted algorithm of [24] is a benchmark optimization technique utilized in this work. The algorithm exploits a coarse-discretization model R_{cd} and an auxiliary kriging interpolation model R_s. The optimization flow can be summarized as follows.

1. *Design space reduction.* Set the lower/upper bounds of the design space X_0 as $l = \min\{x^{*(1)}, x^{*(2)}, \ldots, x^{*(N_{obj})}\}$ and $u = \max\{x^{*(1)}, x^{*(2)}, \ldots, x^{*(N_{obj})}\}$, where $x^{*(k)} = \text{argmin}\{x : F_k(R_{cd}(x))\}$ are extreme Pareto-optimal designs obtained through single-objective optimization runs.

2. *Surrogate model construction.* Allocate training data samples within X_0, acquire R_{cd} simulation data, and identify kriging interpolation model R_s.

3. *Obtaining initial Pareto set.* Optimize R_s using multi-objective evolutionary algorithm (MOEA) [24].

4. *Design refinement.* For K selected designs $x_s^{(k)}$, $k = 1, \ldots, K$, obtain refined (high-fidelity-level) design $x_f^{(k)}$ as

$$x_f^{(k)} = \arg \min_{\substack{x, F_2(x) \leq F_2(x_s^{(k)}) \\ \vdots \\ F_{N_{obj}}(x) \leq F_{N_{obj}}(x_s^{(k)})}} F_1\left(R_s(x) + [R_f(x_s^{(k)}) - R_s(x_s^{(k)})]\right) \tag{1}$$

The refinement procedure (1) can be iterated. Normally, two to three iterations are needed for convergence.

The algorithm described above enables considerable design speedup. As indicated in the literature, a typical cost of MOO is a few hundred of high-fidelity model evaluations [23], [24]). The segmentation technique described in the next section allows for further reduction of the computational complexity.

3. Generalized Design Space Segmentation

Graphical illustration of the original concept of design space segmentation (defined for two-objective case [26]) has been illustrated in Fig. 1(a). The size vector of the search space X_0 is defined as $d^{(1)} = [d_1^{(1)} \ d_2^{(1)} \ \ldots \ d_n^{(1)}]^T = |x^{*(1)} - x^{*(2)}|$, which allows us

to calculate the volume of X_0 as $V_0 = \prod_{k=1,\ldots,n} d_k^{(1)}$. By introducing one intermediate point $\boldsymbol{x}_I^{(1)}$, two reduced sub-domains are created, $X_{1.1}$ and $X_{1.2}$ with the volumes of $V_{1.l} = \prod_{k=1,\ldots,n} d_k^{(I.l)}$, where $\boldsymbol{d}^{(I.1)} = [d_1^{(I.1)} \ldots d_n^{(I.1)}]^T = |\boldsymbol{x}^{*(1)} - \boldsymbol{x}_I^{(1)}|$, and $\boldsymbol{d}^{(I.2)} = [d_1^{(I.2)} \ldots d_n^{(I.2)}]^T = |\boldsymbol{x}^{*(2)} - \boldsymbol{x}_I^{(1)}|$. The intermediate point is generated by solving a single-objective optimization sub-problem

$$\boldsymbol{x}_I^{(1)} = \arg \min_{\boldsymbol{x},\, F_2(\boldsymbol{x}) \leq F_{2.I}^{(1)}} F_1\left(\boldsymbol{R}_{cd}(\boldsymbol{x})\right) \tag{2}$$

In (2), the value of the threshold $F_{2.I}^{(1)}$ is set to allocate the intermediate point around the center of the Pareto front, i.e., $F_{2.I}^{(1)} = [F_2(\boldsymbol{x}^{*(1)}) + F_2(\boldsymbol{x}^{*(2)})]/2$. The starting point for (2) is $[\boldsymbol{x}^{*(1)} + \boldsymbol{x}^{*(2)}]/2$ which is a good approximation of $\boldsymbol{x}_I^{(1)}$ assuming that the Pareto front curvature is limited (which is usually the case for antenna elements). Consequently, the cost of solving (2) is low.

This concept can be generalized to an arbitrary number K of intermediate points $\boldsymbol{x}_I^{(l)}$, $l = 1, \ldots, K$. In this case, the points created along with $K + 1$ sub-domains $X_{K.l}$, $l = 1, \ldots, K + 1$ of the volumes $V_{K.l} = \prod_{k=1,\ldots,n} d_k^{(I.l)}$, where $\boldsymbol{d}^{(I.1)} = |\boldsymbol{x}^{*(1)} - \boldsymbol{x}_I^{(1)}|$, $\boldsymbol{d}^{(I.l)} = |\boldsymbol{x}_I^{(l-1)} - \boldsymbol{x}_I^{(l)}|$ for $l = 2, \ldots, K$, and $\boldsymbol{d}^{(I.K+1)} = |\boldsymbol{x}^{*(2)} - \boldsymbol{x}_I^{(K)}|$. We have $\boldsymbol{x}_I^{(l)} = \text{argmin}\{\boldsymbol{x} : F_1(\boldsymbol{R}_{cd}(\boldsymbol{x})),\ F_2(\boldsymbol{x}) \leq F_{2.I}^{(l)}\}$, where $F_{2.I}^{(l)} = (1 - \alpha_l)F_2(\boldsymbol{x}^{*(1)}) + \alpha_l F_2(\boldsymbol{x}^{*(2)})$, $\alpha_l = l/K$.

The most important advantage of segmentation is dramatic reduction of the overall volume of the concatenated sub-domains as compared to the volume of the original domain X_0. In other words, $V_K = V_{K.1} + \ldots + V_{K.K+1}$ is much smaller than V_0 (cf. [26] for details). Clearly, the benefit is reduction of the number of training samples necessary to build the kriging model (set up independently for each segment). It should be emphasized that although the volume ratio V_0/V_K increases with K, the cost of identifying the intermediate point has to be taken into account as well. Therefore, for

typical two-objective antenna problems, the optimum choice of the number of intermediate points (the point of view of the overall cost reduction) is two or three.

In this work, a generalized domain segmentation is proposed that allows for handling an arbitrary number of design objectives. The concept has been graphically explained in Fig. 1(b) assuming a three-objective case. For a two-fold segmentation, one needs three intermediate points $x_I^{(1.2)}$, $x_I^{(1.3)}$, $x_I^{(2.3)}$, which results in four segments covering the entire Pareto set. The points are obtained as ($k, j = 1, 2, 3, k < j$)

$$x_I^{(k.j)} = \arg \min_{x, F_j(x) \leq F_{j.I}^{(1)}} F_k\left(\boldsymbol{R}_{cd}(x)\right) \tag{3}$$
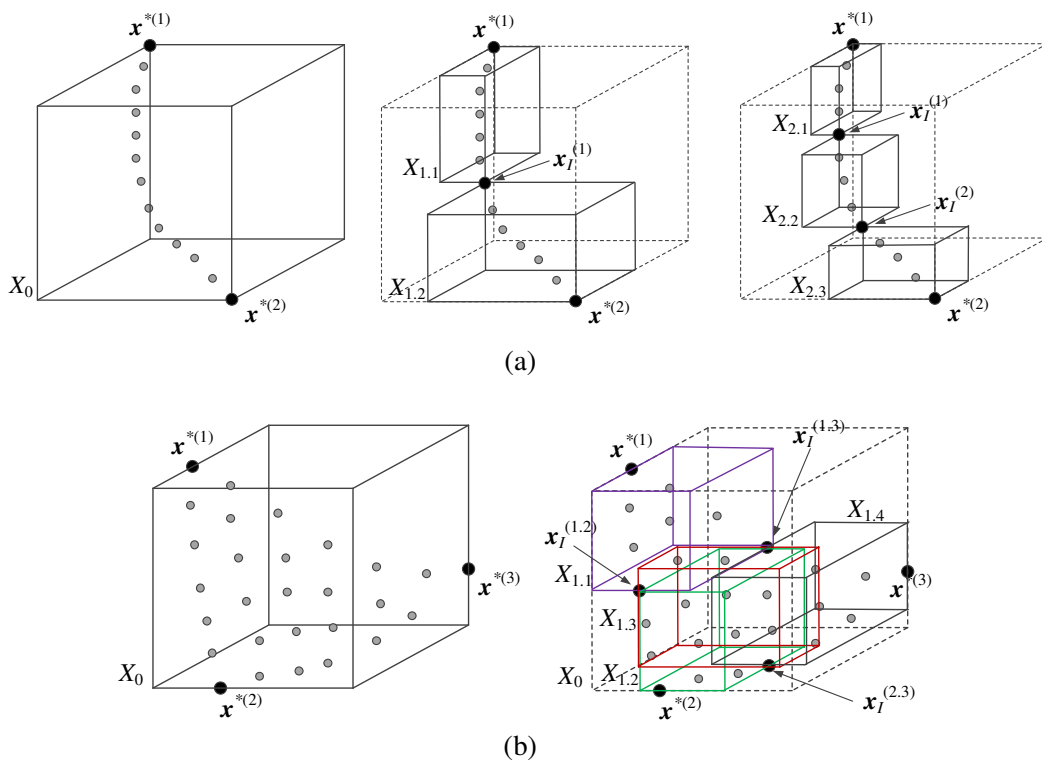

(a)

(b)

Fig. 1. The concept of design space segmentation (illustrated for three-dimensional design space): (a) two design objectives: three cases shown with no segementation, two-fold, and three-fold segmentation, (b) three design objectives: two cases shown with no segmentation and two-fold segmentation. The overall volume of the segments is smaller than the volume of the original space and the benefits increase with the number of segments. Generalization for higher number of objectives is straightforward.

Similarly as before, the intermediate points are obtained through single-objective optimization. However, one needs to consider pairs of objectives and optimize one of them while imposing an acceptance threshold on the second one, and disregarding the third. This way, one can relocate the intermediate points to the boundaries of the Pareto front. For three objectives and two-fold segmentation, there are three intermediate points. Three-fold (and higher-order) segmentation can be defined analogously. We omit the details due to complexity of the notation. Generalized segmentation for a larger number of objectives (beyond three) can be defined in a similar manner. For example, in case of four objectives, two-fold segmentation has four intermediate points and five segments.

4. Demonstration Example and Results

In order to illustrate the operation and performance of the generalized segmentation let us consider an ultra-wideband (UWB) monopole antenna shown in Fig. 2 [27]. The structure features two radiator slots and an elliptical slit below the feed line, both incorporated to achieve a smaller footprint. The antenna is implemented on an FR4 substrate (ε_r = 4.3, h = 1.55 mm, $\tan\delta$ = 0.02). The independent design variables are $\boldsymbol{x}$ = [L_g L_0 L_s W_s d dL d_s dW_s dW a b]^T; W_0 = 2.0. The unit for all dimensions is mm. In the design process, two full-wave EM models are utilized, both implemented in CST Microwave Studio [28] and simulated its time-domain solver. The primary (high-fidelity) model $\boldsymbol{R}_f$ contains about 2,200,000 mesh cells, and its simulation time is 15 minutes on a 2.1 GHz Intel Xeon E5 processor with 64 GB RAM. The low-fidelity model $\boldsymbol{R}_c$ contains 160,000 cells and simulates in 40 seconds. The SMA connector is included in both models to ensure reliability of antenna evaluation.
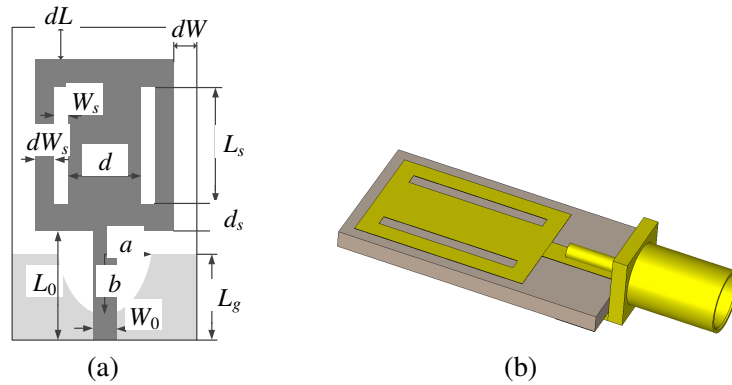
Fig. 2. UWB monopole antenna with elliptical slit below the feed line: (a) top view, (b) 3D view. The ground plane marked with light-gray shade.

In the design process, the following three objectives are considered:

- F_1 – minimization of reflection in 3.1 GHz to 10.6 GHz band,

- F_2 – minimization of antenna footprint (defined as $A(\boldsymbol{x}) = (2dW + 2dW_s + 2W_s + d)(L_0 + 2d_s + L_s + dL))$,

- F_3 – minimization of realized gain variability within UWB frequency range (gain variability is understood as the difference between the maximum and minimum gain within the UWB frequency range).

Furthermore, only the designs for which the maximum in-band reflection does not exceed–10 dB are considered acceptable.

The extreme Pareto-optimal designs have been found using trust-region gradient search [29], [30]. These are $\boldsymbol{x}_1^* = [8.86\ 12.96\ 9.39\ 0.35\ 3.89\ 6.46\ 1.22\ 1.58\ 2.58\ 0.33\ 0.55]^T$, $\boldsymbol{x}_2^* = [9.27\ 13.20\ 8.90\ 0.25\ 3.29\ 0.00\ 0.70\ 1.46\ 0.72\ 0.67\ 0.61]^T$, and $\boldsymbol{x}_3^* = [8.38\ 12.82\ 9.89\ 0.65\ 3.84\ 14.99\ 1.54\ 1.68\ 2.65\ 0.39\ 0.55]^T$. Consequently, the lower/upper bounds of X_0 are $\boldsymbol{l}^* = [8.38\ 12.82\ 8.9\ 0.25\ 3.29\ 0.0\ 0.7\ 1.46\ 0.72\ 0.33\ 0.55]^T$ and $\boldsymbol{u}^* = [9.27\ 13.2\ 8.89\ 0.65\ 3.89\ 14.99\ 1.54\ 1.68\ 2.65\ 0.67\ 0.61]^T$.

The three intermediate points have then been obtained using (3) as follows: $x_I^{(1.2)}$ = [9.12 13.04 8.79 0.29 3.43 2.91 0.87 1.38 1.48 0.53 0.57]^T, $x_I^{(1.3)}$ = [8.72 12.8 9.53 0.51 3.95 11.36 1.33 1.61 2.5 0.35 0.54]^T, $x_I^{(2.3)}$ = [8.8 12.99 9.42 0.45 3.59 7.25 1.1 1.57 1.6 0.54 0.57]^T. The ratio of the volume V_0 of X_0 and the combined volume V_1 of the four segments $X_{1,j}$ (cf. Fig. 1(b)) is around 10^2. The kriging model $\boldsymbol{R}_s$ constructed in X_0 requires 843 data samples (average RMS error of 2.5 percent). The total number of samples required to establish the kriging models in $X_{1,j}$ is $10^3 + 8^3 + 6^3 + 12^3 = 372$ (average errors of 2.4, 2.5, 2.1, and 2.5 percent, respectively). This represents noticeable savings.

The initial Pareto set obtained by optimizing the kriging surrogate using MOEA (Step 3 of the MO procedure of Section 2) has been shown in Fig. 3 along with the Pareto set found in the segmented space. In case of segmentation, individual Pareto fronts obtained within the search space segments have been concatenated and non-dominated designs have been selected in order to obtain the overall Pareto set. It should be noted that both Pareto sets (i.e., obtained with and without segmentation) are similar to each other especially concerning their span within the feature space. This indicates that, for the considered structure, segmentation does not result in Pareto front quality degradation. At the same time, the cost of MO is smaller when using design segmentation as indicated in Table 1.

The final (high-fidelity) Pareto set obtained using the methodology of Section 2 with design segmentation has been shown in Fig. 4. Table 2 gathers antenna dimensions for high-fidelity Pareto-optimal designs. Reflection and realized gain characteristics for the selected designs have been shown in Figs. 4 and 5.
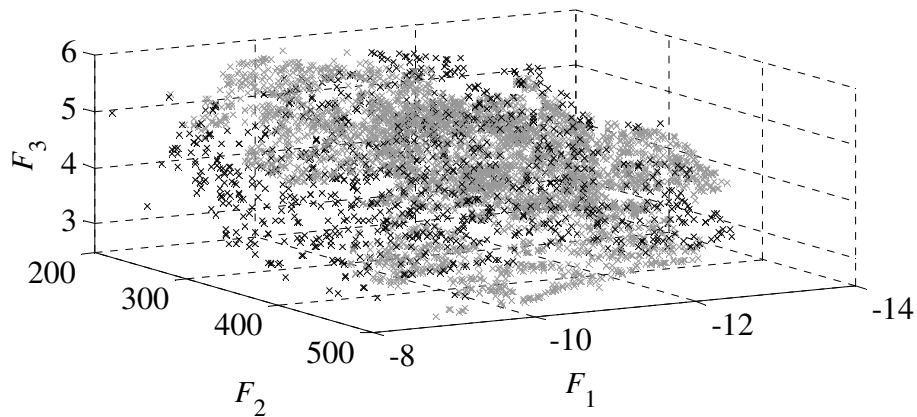
Fig. 3. Pareto set representations found in the original design space X_0 (black) and in the segmented space (gray).
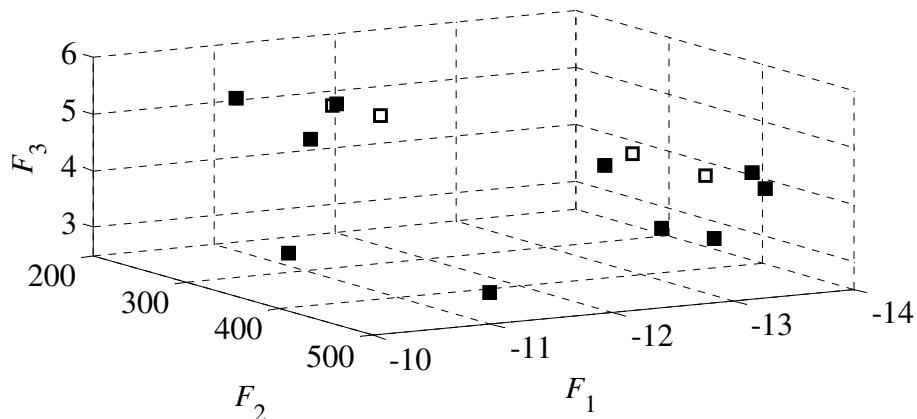

Fig. 4. Refined (high-fidelity) Pareto set obtained using design space segmentation. Designs marked using filled squares are listed in Table 2.
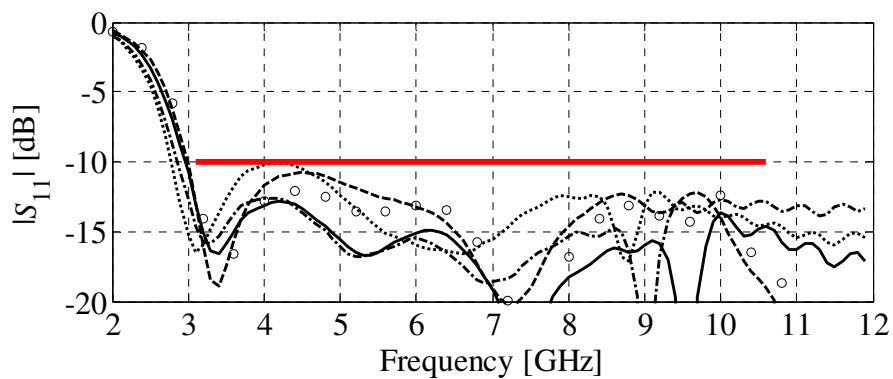

Fig. 5. Reflection responses of the selected high-fidelity Pareto-optimal designs (cf. Table 2): $x_f^{(1)}$ (····), $x_f^{(3)}$ (–·–), $x_f^{(5)}$ (– –), $x_f^{(7)}$ (—), $x_f^{(9)}$ (∘∘).
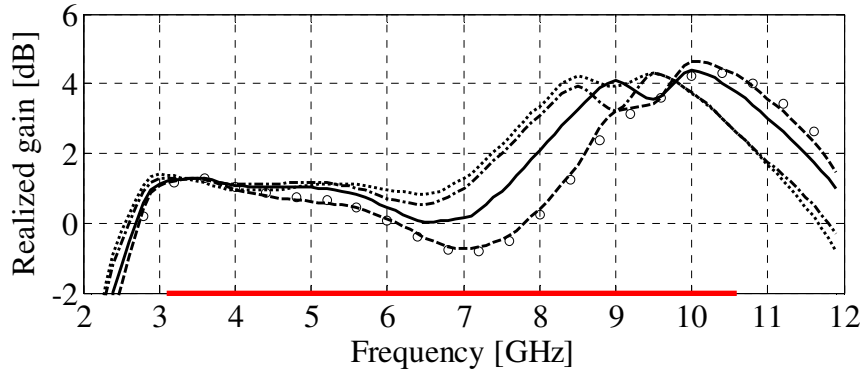
Fig. 6. Realized gain responses of the selected high-fidelity Pareto-optimal designs (cf. Table 2): $\boldsymbol{x}_f^{(1)}$ (····), $\boldsymbol{x}_f^{(3)}$ (–·–), $\boldsymbol{x}_f^{(5)}$ (– –), $\boldsymbol{x}_f^{(7)}$ (——), $\boldsymbol{x}_f^{(9)}$ (○○).

Table 1   Multi-Objective Optimization Cost Breakdown

Cost contributor	No segmentation	Two-fold segmentation
Extreme and intermediate points	347 $\boldsymbol{R}_{cd}$	569 $\boldsymbol{R}_{cd}$
Data acquisition	843 $\boldsymbol{R}_{cd}$	372 $\boldsymbol{R}_{cd}$
MOEA optimization	N/A[*]	N/A[*]
Refinement	45 $\boldsymbol{R}_f$	45 $\boldsymbol{R}_f$
Total cost	97.9 $\boldsymbol{R}_f$ (24.5 h)	86.8 $\boldsymbol{R}_f$ (21.7 h)

[*] The cost of MOEA optimization is negligible as compared to EM simulation (both low- and high-fidelity).

Table 2   High-Fidelity Pareto-Optimal Designs

	Pareto-optimal design									
	$\boldsymbol{x}^{(1)}$	$\boldsymbol{x}^{(2)}$	$\boldsymbol{x}^{(3)}$	$\boldsymbol{x}^{(4)}$	$\boldsymbol{x}^{(5)}$	$\boldsymbol{x}^{(6)}$	$\boldsymbol{x}^{(7)}$	$\boldsymbol{x}^{(8)}$	$\boldsymbol{x}^{(9)}$	$\boldsymbol{x}^{(10)}$
F_1	−10.1	−13.7	−12.6	−11.0	−10.8	−12.9	−12.9	−11.0	−11.5	−13.7
F_2	400	428	476	298	253	497	380	496	261	446
F_3	3.5	4.3	3.7	4.8	5.4	3.6	4.4	3.0	5.1	4.1
L_g	8.60	9.00	8.77	8.90	9.14	8.80	8.93	8.57	9.19	9.07
L_0	12.81	12.92	12.85	12.88	13.07	12.84	12.83	12.88	13.02	12.94
L_s	9.86	9.22	9.53	9.15	9.26	9.47	8.92	9.64	8.99	9.15
W_s	0.57	0.43	0.58	0.44	0.36	0.52	0.50	0.61	0.39	0.51
d	3.85	3.71	3.83	3.62	3.50	3.88	3.84	3.89	3.53	3.75
dL	8.44	9.31	11.61	2.91	1.86	12.67	7.93	13.76	2.30	11.25
d_s	1.34	1.09	1.14	1.29	0.79	1.10	0.95	1.38	0.72	1.08
dW_s	1.63	1.56	1.64	1.60	1.46	1.64	1.56	1.64	1.49	1.52
dW	1.80	2.51	2.43	1.57	1.33	2.58	2.03	2.16	1.42	2.38
a	0.44	0.35	0.36	0.44	0.55	0.35	0.44	0.37	0.53	0.38
b	0.56	0.55	0.56	0.56	0.59	0.56	0.55	0.56	0.60	0.55

Three selected designs, namely, $x^{(1)}$, $x^{(5)}$, and $x^{(9)}$, have been fabricated and measured. Figure 7 shows the photographs of the antenna prototypes, whereas Figs. 8 through 11 show the reflection, realized gain, efficiency, as well as H-plane and E-plane patterns. The agreement between simulation and measurement data is acceptable. The most noticeable differences occur in case of E-plane patters, which is due to the shadowing effect of the 90-degree bend utilized to mount the antenna.
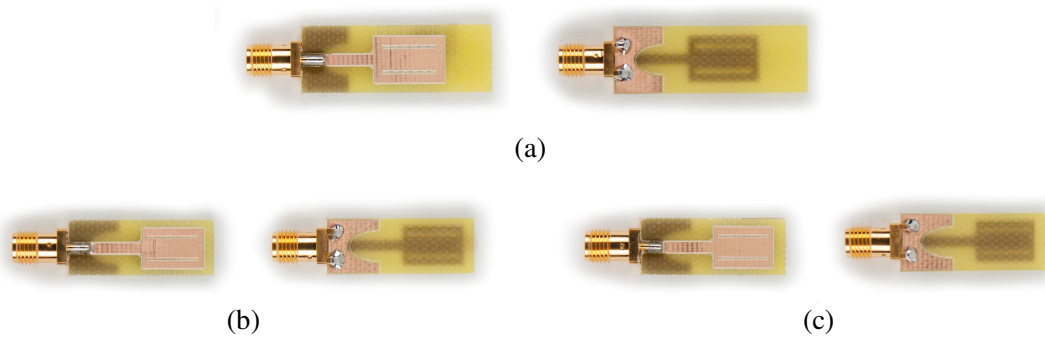

(a)

(b)   (c)

Fig. 7. Photographs of the fabricated antenna prototypes: (a) $x^{(1)}$, (b) $x^{(5)}$, (c) $x^{(9)}$.

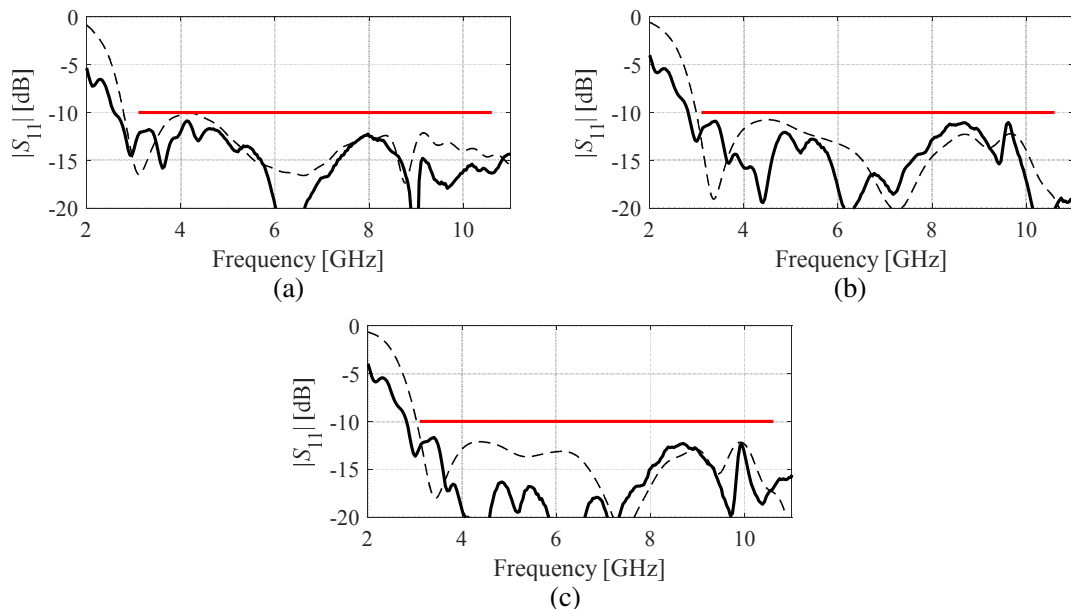(a)   (b)

(c)

Fig. 8. Simulated (- - -) and measured (——) reflection characteristics of the Pareto-optimal antenna prototypes: (a) $x^{(1)}$, (b) $x^{(5)}$, (c) $x^{(9)}$. The horizontal line denotes acceptance level for $|S_{11}|$ of −10 dB.
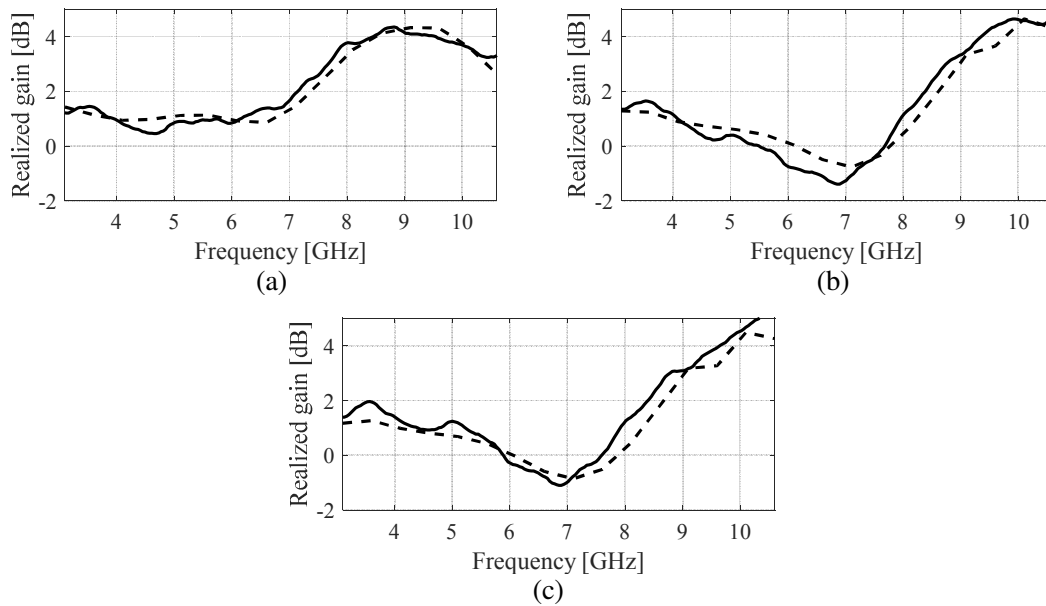
(a)

(b)

(c)

Fig. 9. Simulated (- - -) and measured (——) realized gain characteristics of the Pareto-optimal antenna prototypes: (a) $x^{(1)}$, (b) $x^{(5)}$, (c) $x^{(9)}$.
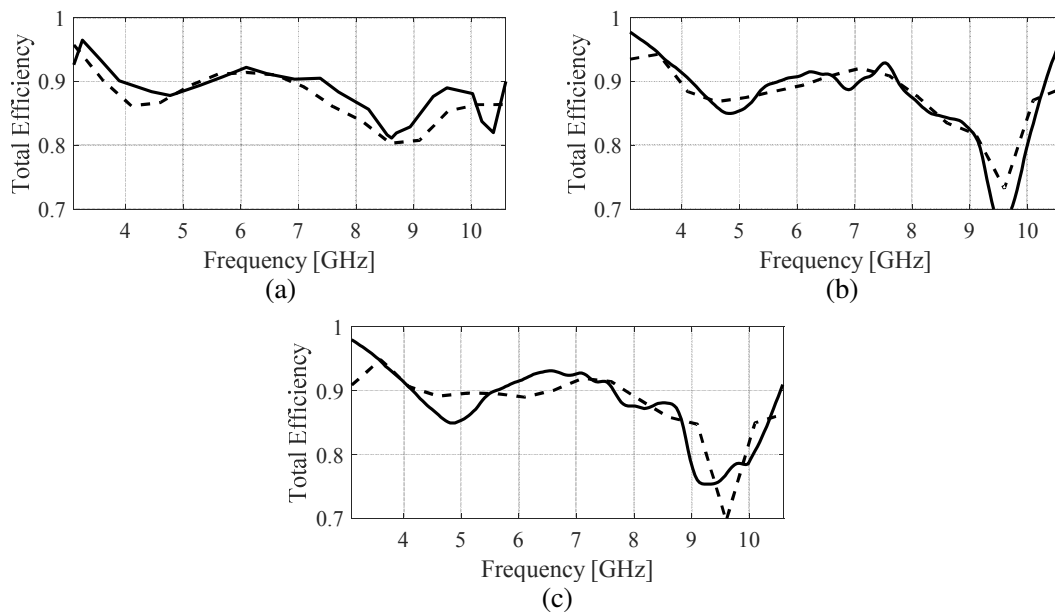

(a)

(b)

(c)

Fig. 10. Simulated (- - -) and measured (——) total efficiency characteristics of the Pareto-optimal antenna prototypes: (a) $x^{(1)}$, (b) $x^{(5)}$, (c) $x^{(9)}$.

It should also be noted that antenna efficiency is quite good (around 90% up to around 7 GHz with a drop to around 80% for upper part of the UWB range) considering a high-loss substrate utilized for structure realization (tanδ = 0.02). Furthermore, neither antenna efficiency nor the radiation patterns change considerably across the Pareto front, in particular, the structure retains its desired characteristics (e.g., omnidirectional radiation).
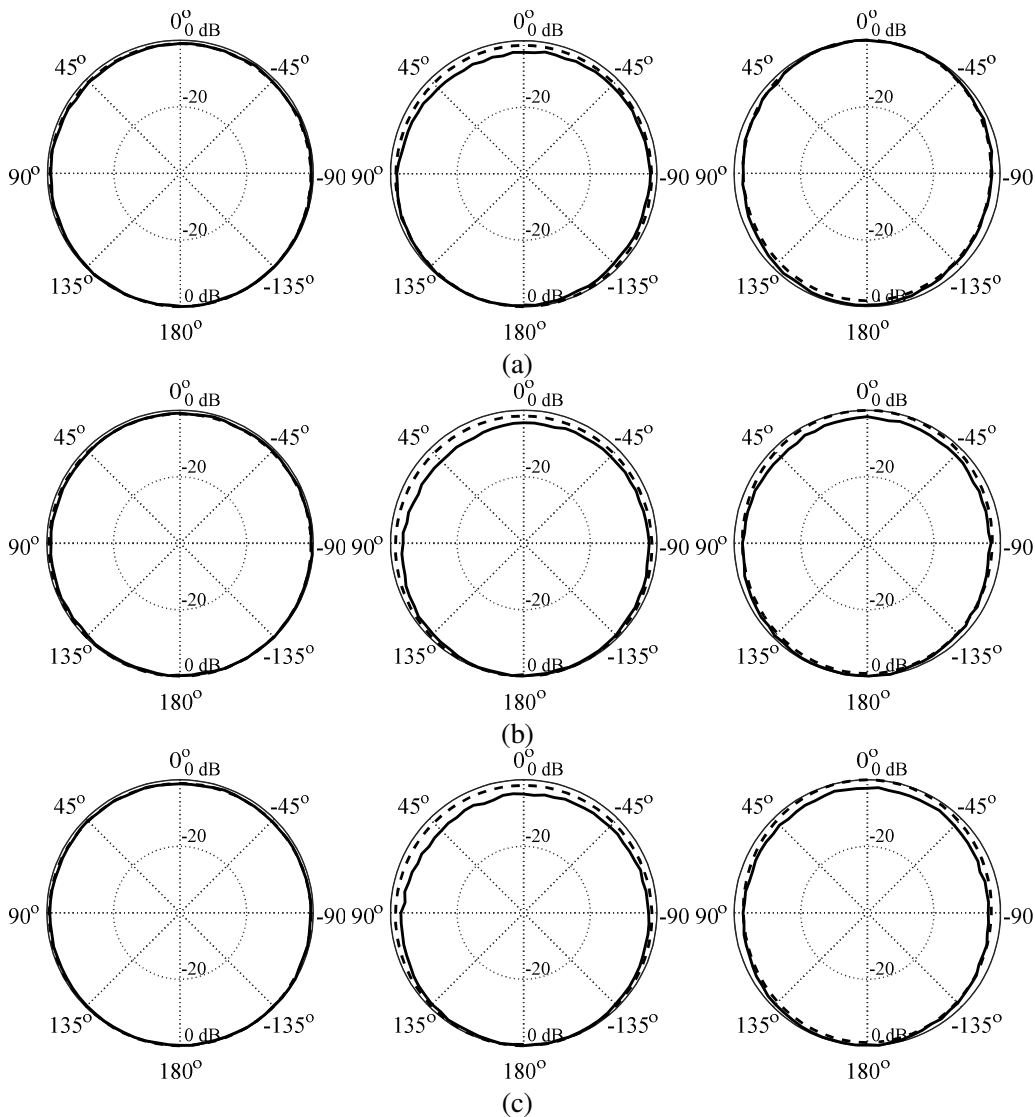

Fig. 11. Simulated (- - -) and measured (——) H-plane patterns of the Pareto-optimal antenna prototypes: (a) $x^{(1)}$, (b) $x^{(5)}$, (c) $x^{(9)}$. From left to right: 4 GHz, 6 GHz, and 8 GHz.
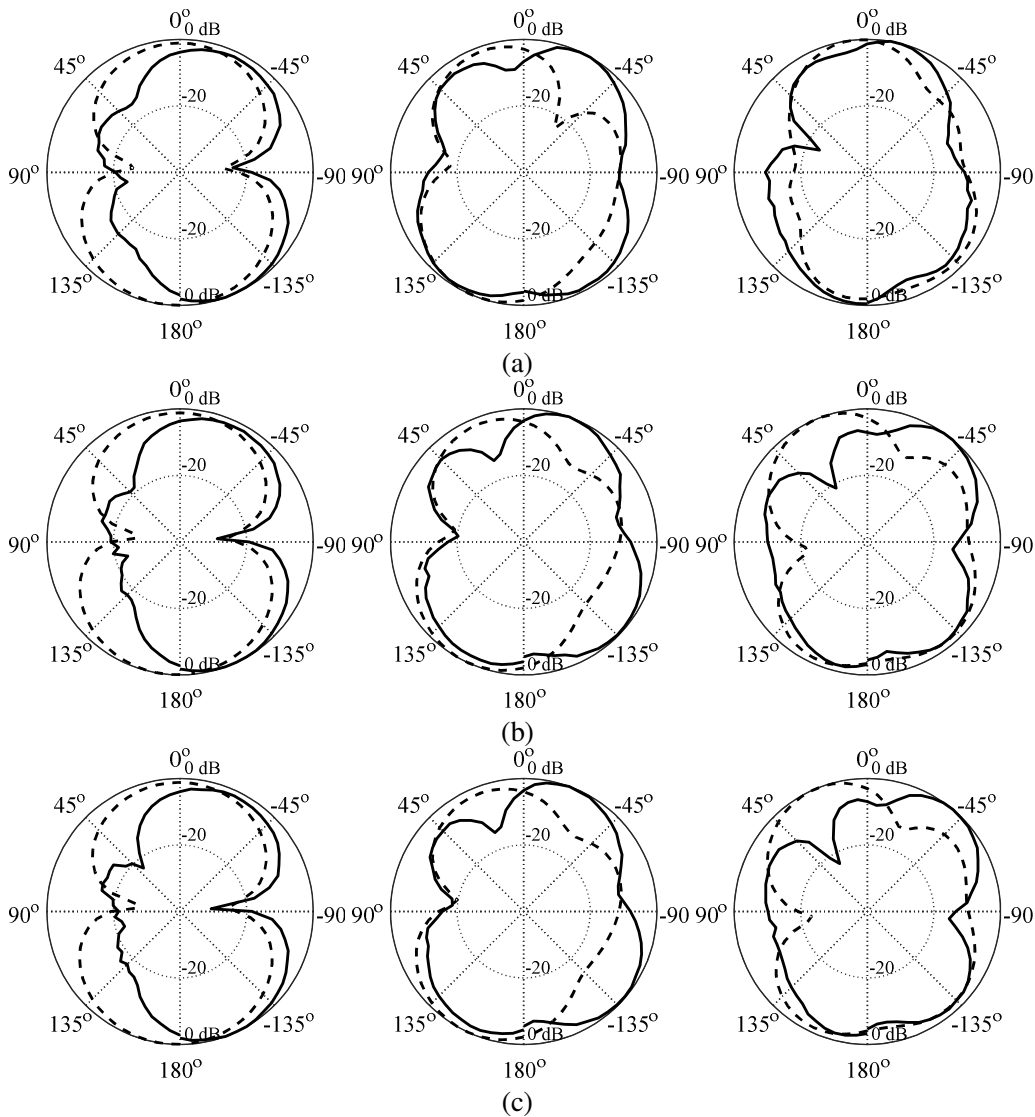
Fig. 12. Simulated (- - -) and measured (—) E-plane patterns of the Pareto-optimal antenna prototypes: (a) $x^{(1)}$, (b) $x^{(5)}$, (c) $x^{(9)}$. From left to right: 4 GHz, 6 GHz, and 8 GHz.

5. Conclusion

The paper presented a generalized design space segmentation technique aimed at accelerating multi-objective optimization of antennas. The discussed method permits considerable reduction of the number of training data samples required to construct the kriging surrogate model utilized to yield an initial representation of the Pareto front. Generalized segmentation works for an arbitrary number of design objectives. For the

sake of illustration, a UWB monopole antenna has been optimized with respect to three goals concerning reflection response, realized gain, and the structure footprint. As compared to conventional (also surrogate-assisted) approach, segmentation leads to over 20 percent reduction of the computational cost of the initial Pareto set generation. Selected Pareto-optimal designs have been fabricated and measured for additional validation.

References

[1] S. Nikolaou and M. A. B. Abbasi, "Design and development of a compact UWB monopole antenna with easily-controllable return loss," *IEEE Trans. Ant. Propag.*, vol. 65, no. 4, pp 2063-2067, 2017.

[2] J. Liu, K.P. Esselle, S.G. Hay, and S. Zhong, "Effects of printed UWB antenna miniaturization on pulse fidelity and pattern stability," *IEEE Trans. Ant. Prop.*, vol. 62, no. 8, pp 3903-3910, 2014.

[3] A. Bekasiewicz and S. Koziel, "Structure and computationally-efficient simulation-driven design of compact UWB monopole antenna," *IEEE Antennas and Wirel. Propag. Lett.*, vol. 14, pp. 1282–1285, 2015.

[4] M.A. Haq and S. Koziel, "A novel miniaturized uwb monopole with five-section stepped-impedance feed line," *Microwave Opt. Tech. Lett.*, 2017.

[5]   L. Li, S.W. Cheung, and T.I. Yuk, "Compact MIMO antenna for portable devices in UWB applications," *IEEE Trans. Antennas Prop.*, vol. 61, no. 8, pp. 4257–4264, 2013.

[6]   M. N. Shakib, M. Moghavvemi, and W. N. L. Mahadi, "Design of a compact planar antenna for ultra-wideband operation," *Applied Computational Electromagnetics Society Journal*, vol. 20, no. 2, pp 222-229, 2015.

[7]   M. Manohar, R. S. Kshetrimayum, and A. K. Gogoi, "Printed monopole antenna with tapered feed line, feed region and patch for super wideband applications," *IET Microw. Antennas propag.*, vol. 8, Iss. 1, pp 39-45, 2014.

[8]   B. Tian, Z. Li, C. Wang, "Boresight gain optimization of an UWB monopole antenna using FDTD and genetic algorithm," *IEEE Int. Conf. Ultra-Wideband*, pp. 1-4, 2010.

[9]   Z. Yang, J. Zhou, H. Li, W. Li, X. Shi, and M. Wang, "Design of hexagonal circularly polarized antenna array using paralleled dynamic minimum lower confidence bound," *Int. J. RF & Microwave CAE*, available online, 2017.

[10]   J. Nocedal, S.J. Wright, *Numerical Optimization*, Springer, 2006.

[11]   X.-S. Yang, K.-T. Ng, S.H. Yeung, and K.F. Man, "Jumping genes multiobjective optimization scheme for planar monopole ultrawideband antenna," *IEEE Trans. Antennas Prop.*, vol. 56, no. 12, pp. 3659-3666, 2008.

[12]   D. Ding and G. Wang, "Modified multiobjective evolutionary algorithm based on decomposition for antenna design," *IEEE Trans. Antennas Prop.*, vol. 61, no. 10, pp. 5301-5307, Oct. 2013.

[13]   S. Chamaani, S.A. Mirtaheri, and M.S. Abrishamian, "Improvement of time and frequency domain performance of antipodal Vivaldi antenna using multi-objective particle swarm optimization," *IEEE Trans. Antennas Prop.*, vol. 59, no. 5 pp. 1738-1742, May 2011.

[14]   R. Ghatak, A. Karmakar, and K.R. Poddar, "Evolutionary optimization of Haferman carpet fractal patterned antenna array," *Int. J. RF & Microwave CAE*, vol. 25, no. 8, pp. 719-729, 2015.

[15] M. Ghassemi, M. Bakr, and N. Sangary, "Antenna design exploiting adjoint sensitivity-based geometry evolution," *IET Microwaves Ant. Prop.*, vol. 7, no. 4, pp. 268-276, 2013.

[16] S. Koziel and A. Bekasiewicz, "EM-simulation-driven design optimization of compact microwave structures using multi-fidelity simulation models and adjoint sensitivities," *Int. J. RF & Microwave CAE*, vol. 26, no. 5, pp. 442-448, 2016.

[17] S. Koziel, and S. Ogurtsov, *Antenna design by simulation-driven optimization*, Springer, New York, 2014.

[18] A. Bekasiewicz and S. Koziel, "Precise control of reflection response in bandwidth-enhanced planar antennas," *Int. J. RF Microwave CAE*, vo. 26, no. 8, pp. 653-659, 2016.

[19] S. Koziel and A. Bekasiewicz, "Expedited simulation-driven design optimization of UWB antennas by means of response features," *Int. J. RF and Microwave CAE*, vol. 27, no. 6, 2017.

[20] S. Koziel and A. Bekasiewicz, "Computationally feasible narrow-band antenna modeling using response features," *Int. J. RF & Microwave CAE*, vol. 27, no. 4, 2017.

[21] N.V. Queipo, R.T. Haftka, W. Shyy, T. Goel, R. Vaidynathan, and P.K. Tucker, "Surrogate-based analysis and optimization," *Prog. Aerospace Sci.*, vol. 41, no. 1, pp. 1-28, Jan. 2005.

[22] K. Deb., *Multi-objective optimization using evolutionary algorithms*, New York: John Wiley & Sons, 2001.

[23] S. Koziel and S. Ogurtsov, "Multi-objective design of antennas using variable-fidelity simulations and surrogate models," *IEEE Trans. Antennas Prop.*, vol. 61, no. 12, pp. 5931-5939, Dec. 2013.

[24] S. Koziel, and A. Bekasiewicz, "Low-cost multi-objective optimization and experimental validation of UWB MIMO antenna," *Eng. Comp.*, vol. 33, no. 4, pp. 1246-1268, 2016.

[25] S. Koziel and A. Bekasiewicz, "Computationally efficient two-objective optimization of compact microwave couplers through corrected domain patching," *Metrology and Measurement Systems*, 2017.

[26] S. Koziel, A. Bekasiewicz, Q.S. Cheng, and S. Li, "Accelerated multi-objective design optimization of antennas by surrogate modeling and domain segmentation," *IEEE European Ant. Prop. Conf.*, 2017.

[27] M.A. Haq, S. Koziel, and Q.S. Cheng, "EM-driven size reduction of UWB antennas with ground plane modifications," *Int. Applied Computational Electromagnetics Society (ACES China) Symposium*, 2017.

[28] CST Microwave Studio, ver. 2016. CST AG, Bad Nauheimer Str. 19, D-64289 Darmstadt, Germany, 2016.

[29] A. Conn, N.I.M. Gould, P.L. Toint, *Trust-region methods*, MPS-SIAM Series on Optimization, Philadelphia, 2000.

[30] S. Koziel and A. Bekasiewicz, "Rapid design optimization of multi-band antennas by means of response features," *Metrology and Measurement Systems*, vol. 24, no. 2, pp. 337-346, 2017.